IEEE Access
Multidisciplinary | Rapid Review | Open Access Journal

IEEE POWER & ENERGY SOCIETY SECTION

Received July 23, 2020, accepted July 30, 2020, date of publication August 4, 2020, date of current version August 17, 2020.

Digital Object Identifier 10.1109/ACCESS.2020.3014235

Research on Current Limiting Method Used for Short Circuit Fault Current of Resonant DC Transformer Based on Inverted Displacement Phase Control

CHAORAN ZHUO, (Member, IEEE), XU YANG, (Senior Member, IEEE), XIAOTIAN ZHANG, (Member, IEEE), AND XIONG ZHANG

State Key Laboratory of Electrical Insulation and Power Equipment, Xi'an Jiaotong University, Xi'an 710049, China

Corresponding author: Chaoran Zhuo (chaoranzhuo0208@163.com)

This work was supported by the National Key Research and Development Program of China under Grant: Basic Theory of Fault Current Suppression in Flexible DC Grid. 2018YFB0904600.

ABSTRACT Due to the characteristics of high efficiency and flexible transformation ratio, full-bridge CLLC resonant DC transformers have been increasingly used for DC grid in recent years. Based on the analysis of the working principle of CLLC resonant DC transformer circuit, this article analysis the current gain characteristics by using fundamental wave analysis method, the parameter influences of resonance network frequency and the transformer gain is also being concerned. On the basis of using soft switching method, this article will introduce a method of inverted displacement phase control. The working range will be further refined in the original circuit, and the linear control region will be expanded as well. In this way, the output current will have a precise control under the condition of short circuit, which will satisfy the low voltage ride-through requirements of DC transformers applied to the grid connection of renewable energy. Finally, the method proposed in this article is verified by simulation and hardware-in-the-loop experiment.

INDEX TERMS Resonance, power electronics transformer, short circuit current limit, low voltage ride through, phase shift control.

I. INTRODUCTION

In recent years, DC transmission and distribution systems have attracted the attention of the industry field because of their advantages of large energy capacity, low losses and high-power supply quality [1]. With the deepening of research, the problems caused by the low damping characteristics of the DC power grid are also constantly obvious, especially the fault current limiting problem under short-circuit fault conditions has been more and more paid to attention [2].

In DC grid, DC power electronic transformers can be used to connect the grid between different voltage levels or as a connector between the renewable energy power generation system and the DC grid. In order to improve the transmission efficiency of DC transformers, CLLC resonant converters based on soft-switching resonance type have received more and more attention [3]. This type of resonant converter has natural soft switching characteristics, which can achieve zero voltage turn-on (ZVS) of the primary-side inverter switches and zero current turn-off of the secondary-side rectifier diode at a wide input voltage and full load range (ZCS), which does not require any auxiliary network and is relatively easy to control [4], [6]. There are many studies that have carried out a lot of research work on it, and many articles have studied the application of CLLC resonant converters in bidirectional DC/DC converters. Reference [5] proposes a one-way LLC converter topology. This circuit topology is mainly designed with a resonant topology on the primary side of the converter, but it is only a traditional full-bridge converter when the reverse side of the side is working. Reference [7] proposes an asymmetric bidirectional CLLC resonant converter structure, which realizes soft switching during bidirectional operation. Reference [8] introduces a symmetrical and efficient LLC resonant converter. This symmetric LLC resonant network has self-turn-off device that can realize ZVS and soft-switching capability on both primary and secondary side. Any snubber circuit is required to reduce the voltage stress of the switching device, and the power conversion efficiency

The associate editor coordinating the review of this manuscript and approving it for publication was Elisabetta Tedeschi.

in any direction is exactly the same as each other. However, the gain of its resonance point is less than one and is affected by the load, and the rectifier diode does not achieve ZCS. Reference [9] proposes another bidirectional full-bridge CLLC resonant DC converter. While maintaining the advantages of LLC resonant converter high efficiency and high-power density, it has the ability to transmit energy in both directions without any buffer circuit. Soft switching is realized, however, because the rectifier bridge of the secondary side does not use synchronous rectification technology, the efficiency of the whole machine still has great development potential. Although there are some problems with these circuits, the achievements of these researchers have greatly promoted the efficient application of DC transformers. The principle topology of DC power electronic transformer based on LLC resonant conversion circuit can be seen in Figure 1. The circuit structure has strong modularity, flexible combination, and high controllability. By using ISOP (input series, output parallel) connection, the transformer can connect the medium voltage 10kV and the low voltage 750V DC bus. The efficiency of the entire transformer has now reached more than 97% (silicon devices) or 98% (silicon carbide devices) [10], Due to flexible control, low loss, and high efficiency, many equipment manufacturers have used this topology as the main circuit of DC transformers for production applications. Transformers of this topology play an important role in the field of DC distribution.

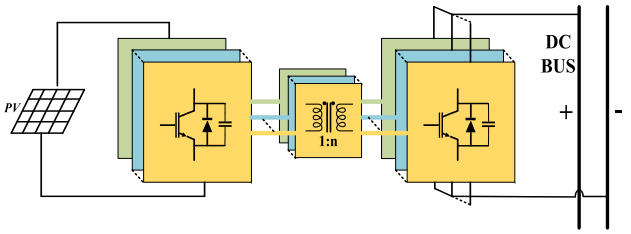

FIGURE 1. Topological structure diagram of DC power electronic transformer based on LLC resonant conversion circuit.

As a connecting element between different voltage levels, the transformer should also take into consideration the fault current limiting and protection in addition to transmitting power. When a short-circuit fault occurs on the external line of the transformer, due to the low impedance of the DC line, a large value of short-circuit inrush current will be generated, which will cause serious damage to the equipment and the line as well. In order to prevent short-circuit and over-current situation, up to now, the industry field mainly uses current limiting inductor with DC circuit breaker placed in series to the transformer output to protect the line and equipment [12]. The current limiting inductor is used to limit the rise rate of the short circuit current when a short circuit fault occurs, and provide a buffer time for the circuit breaker action to cut off the circuit to achieve the purpose of line protection [11]. Regardless of other factors such as cost, this current-limiting protection scheme is sufficient to protect the safety of equipment and transmission lines [13]. However, as more and more renewable energy power generation systems are connected to the DC system, these grid-connected devices must provide low voltage ride-through functions [14]. The current-limiting protection scheme described above is obviously unable to meet the system requirements. At this time, outputting a controllable output current is one of the necessary functions of power electronic transformers [15].

Based on the above requirements, this article has researched in depth on the current limiting control method of DC power electronic transformer using CLLC resonant converter circuit. On one hand, the design and optimization of the resonance parameters must meet the high-efficiency transmission requirements of the symmetrical CLLC resonant conversion circuit under ZVS and ZCS conditions, that is, the converter must meet the gain characteristics and soft switching realization conditions [16]–[18]. On the other hand, the low voltage ride-through requirement needs a precise control to the output current from transformer in case of short circuit happen. Many researchers have had a lot of investigation on DAB circuit and its derivatives. By doing improvements on the topologies of the resonance circuit and relating control algorithms, the circuit can work on default working point. By this way, ZVS can be realized together with the better performance on working efficiency improvements [19]. With the expansion of application scope and development of DC system, researchers have found besides to satisfy the high performance of power transmission requirements, system protection has also become to a big issue, furthermore, with the development of renewable energy, some circuit working requirements under abnormal conditions have also been raised. References such as [20] focus on solutions of protection and isolation of DC power distribution network by using active current limiting control, reference [21] which give solutions of large ratio DC/DC transformer with ability of short circuit limitation ability [22], raise up the ideas on modular DC power flow controller with current limiting function, and reference [23] describes current limiter characteristics and optimal configuration considering DC inductors [24]. All these references are referring to the researches under various extreme conditions based on traditional DAB circuit. The research in this article is also carried out under this background, focusing on the output current control method of DC transformers for renewable energy under short circuit conditions [25]. Usually, two-phase shift or three-phase shift control is being used because the output current is sensitive to control parameters in DC loop when current changed rapidly. However, when controlling the system output current, problems of poor linearity and narrow linear working area are raised. In order to improve the control accuracy under short circuit conditions and meanwhile expand the linear working area, an output reverse-phase control method based on inverted displacement phase control method is proposed, so that the transformer can meet the control requirements of the current controllable followed by changing with output voltage during low voltage ride through.

Finally, the correctness of the proposed method is verified by simulation analysis and hardware-in-the-loop experiment.

This article consists of the following parts: Section two focuses on the analysis of the working process of CLLC resonant converter. The third section analyzes the inverted displacement phase control process of the CLLC resonant circuit. Fourth section discusses the active control method of the output current of the power electronic transformer when a short-circuit fault occurs. Section 5 analyzes the simulation results. Finally, Section 6 gives the conclusions.

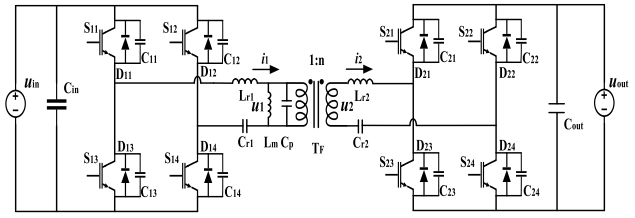

FIGURE 2. Schematic diagram of the topology of the full-bridge CLLC resonant converter module.

II. WORKING PROCESS ANALYZE OF CLLC RESONANT CONVERTER USING REVERSE CURRENT CONTROL

Based on the market's production compliance, electrical isolation is necessary for DC transformers which connected to photovoltaic system. So far, the basic module which constitutes the DC transformer is a full-bridge CLLC resonant converter module. The topology of a bidirectional full-bridge CLLC resonant converter with electrical isolation is shown in Figure 2. Among them, the electrical power semiconductor devices S_{11}-S_{14} and S_{21}-S_{24} constitute two full-bridge converters, L_m is the magnetizing inductance of the high-frequency transformer TF. C_p is the parasitic capacitance between the coil winding layers and turns of the high-frequency transformer TF. L_{r1} and L_{r2} are resonant inductances, including the leakage inductance of the primary and secondary sides of the transformer respectively. C_{r1} and C_{r2} are resonant capacitors and have a DC blocking effect; D_{11}-D_{14}, D_{21}-D_{24} and C_{11}-C_{14}, C_{21}-C_{24} are diodes and capacitors connected in parallel to S_{11}-S_{14} and S_{21}-S_{24}.

As described in previous, many researchers have discussed the working process of the CLLC resonant converter with a lot of research results [1]–[3]. Therefore, this article does not analyze the working principle and control method during normal conversion. Instead, it focuses on output current control of the transformer when a short-circuit fault occurs in the resonant converter. When a short-circuit fault occurs, the line impedance decreases sharply, thus if wants to reduce the transformer output current, the transformer must reduce its output voltage. The working characteristics of DAB module have been changed from voltage source control mode into current source control mode after short circuit happen. When resonance cavity of the transformer's primary side is working in forward direction, S_{11}, S_{14} and S_{12}, S_{13} are pair of complementary drive signals with a controllable duty cycle to achieve the inverter function, and the primary side is shifted into the phase-shifted inverter working mode. After a further analysis to the circuit, control algorithms which are mentioned by current references are mostly aiming to improve the efficiency. Self-shutdown devices in the secondary side are controlled as synchronous rectification mode. The output voltage is only dependent by shift angle in primary side, which causes problems. Because lacking of control parameters, adding small impedance of the circuit itself, it is very difficult to achieve high precise control accuracy and sensitivity to the output current, which make it very difficult to realize the function of low voltage ride trough. In order to solve this problem, basing on cardinal expansion principle, this article proposes to adopt a reverse current control strategy in which the primary and secondary sides are simultaneously shifted and controlled separately. The working mode of secondary side H-bridge is shifting from diode rectifier into phase shift control condition. The short-circuit output current is basically stabilized by phase shift angle in resonance circuit in primary side, then the reverse phase shift angle of the secondary resonance circuit is moved to control the output current accurately. Under this way, it can create a significant improvement to the linearity of output current control and the expansion of adjustment angle as well.

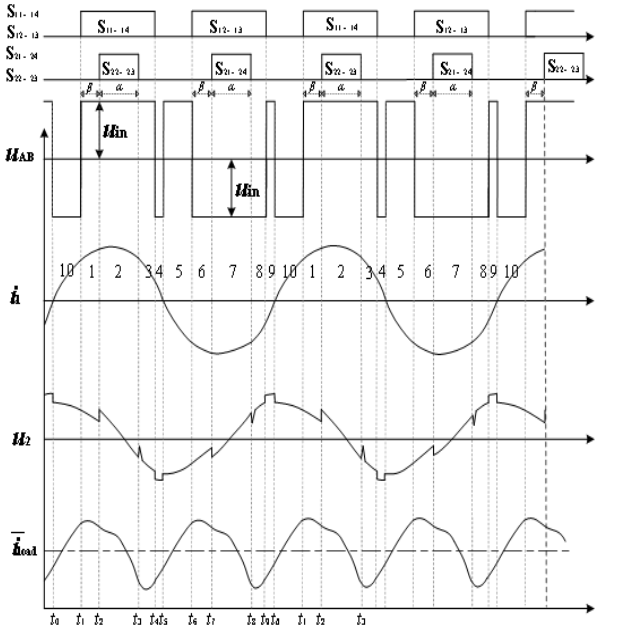

FIGURE 3. The output waveforms of the main electrical parameters of the dual independent phase-shifted CLLC resonant converter.

Based on above analysis, Figure 3 shows the waveform analysis when considering reverse current control. In Figure 3, the PWM waveform of the secondary side rectifier bridge control signal is shown in below. It can be noticed that the trigger phase sequence is different from the general synchronous rectification control, and the phase in this case is 180° shift from the general synchronous rectification control.

There are two kinds of phase shifts corresponds to the drive signals in secondary H-bridge. One is the lagging angle β which relatives to the phase of the primary inverter bridge, and the other is its conduction width α. From the circuit topology point, it can be seen that when the IGBTs of the secondary rectifier bridge is turned on, the direction of the output current is different from the previous moment. Since it is the output reverse current, the average current of the transformer will be reduced. The reduction depends on the angle β and conduction width α. However, these can only change within a certain range. The circuit operation corresponding to each period is shown in Figure 4.

Combined with the working process which is analyzed in Figure 3, it can be seen that a resonance period can be divided into ten parts (see in Figure.4) since secondary side is adding a reverse control. Due to the selection of a suitable angle in the secondary rectifier bridge to incorporate the process of reducing the current, processes 2 and 7 that are not found in the general CLLC resonant circuit. When paying attention to the current direction, lagging angle β and conduction angle α will determine when and how long time the reverse direction current is added. As long as the phases of lagging angle β and conduction angle α are selected properly, the output current can be greatly reduced without changing the phase shift angle γ in primary side. The current control precision and linear working space can be expanded by control angle β and α which can further refine control effect. It can be seen that if the primary side inverter phase-shift control angle is added, there are three variables in the control system that affect the final output of the converter, which lays a solid foundation for the short-circuit current control of the power electric transformer.

III. PHASE VARIABLE INTEVAL AND PARAMETER OPTIMIZATION OF CLLC CIRCUIT

When short-circuit fault occurs in the DC loop, because loop impedance is very small, in order to satisfy the requirement of low voltage ride though within a certain range of output current, it means that the working mode of the DC transformer has been changed from the original voltage source type into current source type and meanwhile have a wide linear working space and high control accuracy. output voltage of the DC transformer is very low and has a wide degree of linear controllability. From the analysis in Section 2, it can be known that, due to the introduction of the two control parameters β and α of the secondary-side rectifier bridge, plus the inverter phase-shift control angle γ of the primary-side rectifier bridge, there are three quantities that can be used to control the final output voltage of the transformer. To achieve the required linearity, sensitivity and stability requirements of the system, these three quantities must be coordinated on the basis of satisfying certain constraints.

It is pointed out in section 2 that the value of the control parameter β is related to the resonance voltage of the LC circuit and the output voltage. The relationship between the control quantities α, β and shift angle of the primary-side inverter bridge γ has become to the key factor of precisely and rapidly output current control. In order to understand the working process of the circuit more clearly, Figure 4 indicates the details in every stages of the circuit, which should pay special attention to the electrical stress of the switches.

It can be seen from the subfigure 1 in Figure 4 that the circuit has the relationship as follows. In stage 1 $[t_1-t_2]$, S_{11} and S_{14} are turned on, u_{AB} is the voltage between point A and B which has the same amplitude with input voltage U_{in}. The current will flow to the secondary rectifier bridge through the transformer T_F. Set the direction of the primary current is positive, the input voltage source U_{in} forces the primary current to move toward S_{14} in the positive direction through S_{11}, forming to a L_{r1}-C_{r1} resonance circuit in primary side. All self-shutdown devices on the secondary side of the transformer are in the off state. The current on the secondary side of the transformer flows through diode D_{21} to the load and returns from diode D_{24}, forming to a L_{r2}-C_{r2} resonance circuit in secondary side.

Stage 2 $[t_2-t_3]$: S_{11} and S_{14} remain on, and the primary side of transformer working state remains unchanged. However, S_{22} and S_{23} in the secondary rectifier bridge are turned on by adding a forward driving voltage. As the direction of the current is the same as the direction of the resonant voltage at this time, the current i_2 flows backward through the load through S_{23} and returns to the resonant circuit from S_{22}, as shown in process 2 of Figure 4.

The process of stage 3 $[t_3-t_4]$ is the same as that of stage 1, and the relationship between the resonance current and the load is the same as stage 1;

In stage 4 $[t_4-t_5]$, due to the phase shift control on the primary side, none of the four IGBTs are turned on. Under the effect of the resonant circuit, the current i_1 continues to flow through the diodes D_{12} and D_{13}, and the voltage u_{AB} across A and B is in amplitude. Same value as U_{in} but opposite direction, $u_{AB} = -U_{in}$

Stage 5 $[t_5-t_6]$, the four IGBTs of the primary inverter bridge in this stage continue to be non-conducting, but under the effect of the resonant circuit, the current i_1 reverses, and the freewheeling diode i_s composed of D_{12} and D_{13} It becomes D_{11} and D_{14} to continue to flow, and the voltage u_{AB} across A and B changes accordingly, $u_{AB} = U_{in}$.

The process of stage 6 $[t_6-t_7]$ -stage 10 $[t_0-t_1]$ is similar to the process of the previous analysis, except that the resonance current is reversed and will be omitted later.

As can be seen from the previous equation (1), before the reverse side current reverse flow control process is introduced, the current in a cycle is determined by the rectified output in stage 1, and the current is flowing to the load and external support the process of capacitor charging; When the secondary side current reverse control process is introduced, in the conduction angle α of S_{22} and S_{23} in the secondary side rectifier bridge, the current is a process of reducing the load current, the length of the reduction time is α, and when it is effective is controlled by the control angle β decision. The relationship between these two parameters and

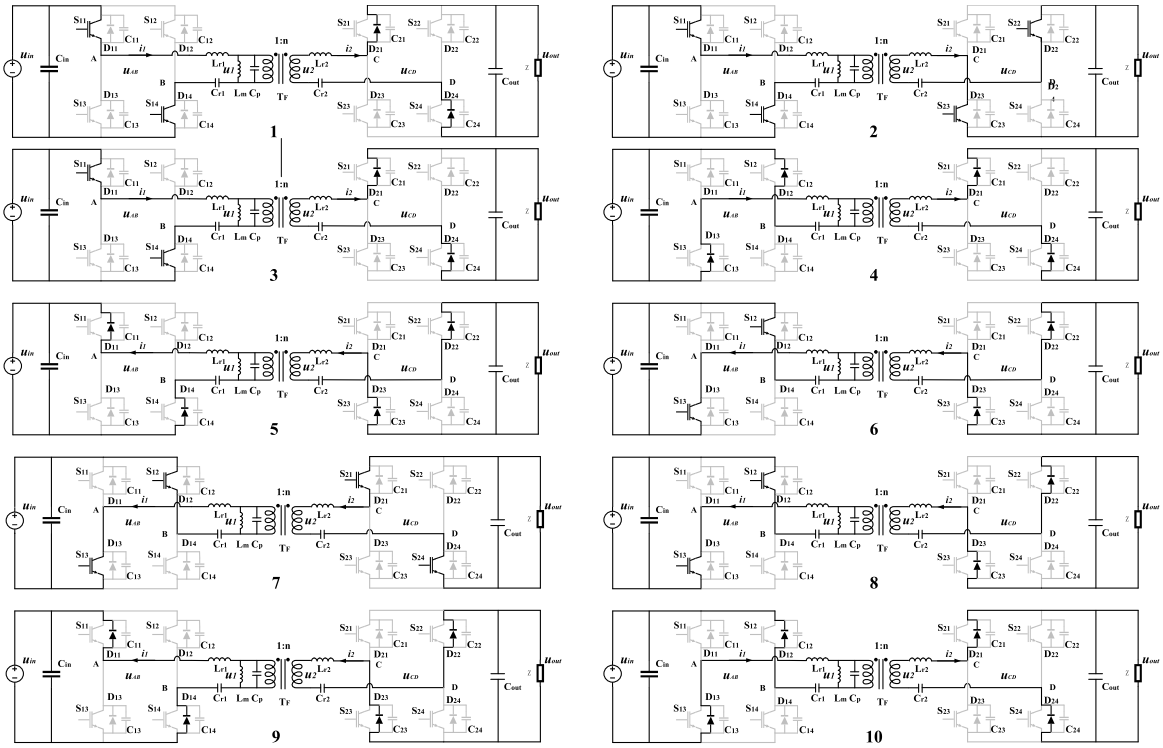

FIGURE 4. Schematic diagram of the double-shift phase coordination control short-circuit output current circuit in each period of conduction.

the output current will determine the current limiting control method.

Equation (1) gives out the average output current I_{dav1} from the converter when without using reverse control method.

$$I_{dav1} = \frac{U_{out}}{Z_L} + \frac{0.9}{(Z_L + Z_{LC2})} \cdot (U_{LC2} + 0.9U_{in} \sin \gamma) \quad (1)$$

Equation (2) gives out the average output current I_{dav2} from the converter when using the reverse control method with lagging angle β and conduction angle α.

$$I_{dav2} = \frac{U_{out}}{Z_L} + \frac{0.9}{(Z_L + Z_{LC2})} \cdot (U_{LC2} + 0.9U_{in} \sin \gamma)(1 + \cos(\beta + \alpha) - \cos \beta) \quad (2)$$

In equations above, where Z_{LC2} is the resonant impedance from the secondary side of the transformer, U_{LC2} is the effective value of resonant voltage, U_{in} is the input voltage and Z_L is the impedance of the short circuit.

Comparing equation (1) and (2), it can be found that by introducing reverse current control, with the conduction of under the same input voltage and phase shift control angle γ, it has a very close relationship between the average output current and control angles.

When keeping fixed value of phase shift angle γ, by selecting proper lagging angle β and conduction angle α, it will provide great benefit to increase control sensitivity and linearity. Figure 5 shows the relationship between the output average current I_{dav2} and α, β at two different γ values. Figure 5a and 5b are represent the situation of $\gamma = 180°$ degree and 90° degree respectively. It can be seen that the

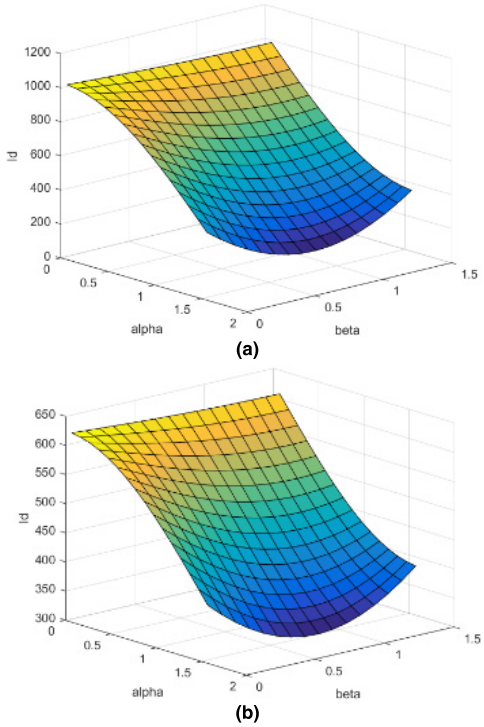

FIGURE 5. The relationship between output current i_{2l} and α, β at different γ. (a) The relationship between output voltage and α, β when $\gamma = 180°$. (b) The relationship between output voltage and α, β when $\gamma = 90°$.

linearly of the output current gradually deteriorates with the increase of the lagging angle β, meanwhile the linear

workspace of conduction angle α is within a certain range, therefore, in order to achieve a good control effect, the three quantities must be coordinated very well.

Another advantage of introducing inverted displacement phase control is the voltage stress reduction of switches when compare with traditional control strategy. Seeing Figure 3 and Figure 4, without inverted control, voltage stress of IGBT switches in the secondary side of the transformer is the summation of peak voltage U_{2m} from secondary side and peak voltage of resonance loop U_{LCr2}. Considering the application redundancy, voltage tolerance of these semiconductor switches is still a problem that cannot be ignored. After introducing reverse control, by controlling the lagging angle β and conducting angle α properly, it is possible to change the area where the peak voltage of $U_{2m}+ U_{LCr2}$ can be turned into conduction area. Therefore, the IGBT switch was originally turned off does not need to withstand the high voltage, which can greatly reduce the voltage stress of the IGBTs in secondary side. This phenomenon can be noticed when see Figure 6 which describes the waveform of the secondary side IGBT voltage stress. From the figure, voltage stress is greatly reduced up to 40% when applying reverse control.

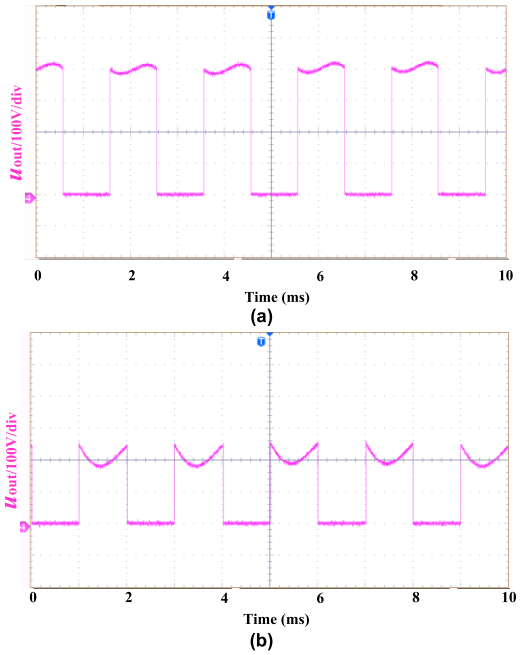

FIGURE 6. The IGBT voltage comparison diagram with and without reverse current control. (a) IGBT voltage comparison diagram without reverse current control. (b) IGBT voltage comparison diagram with reverse current control.

IV. RESEARCH ON TRANSFORMER OUTPUT CURRENT LIMIT CONTROL METHOD

As well known, in normal operation mode of resonance DAB converter, its output is characterized as a voltage source, which stabilize the output voltage in a certain level. When a short circuit happen to the output side, the converter itself needs to have the low voltage ride through ability, that is to maintain a certain output current. The amplitude of this current and the maintenance time are determined according to the short circuit voltage level. In this way, the output voltage of DAB converter is no longer stabile, but to keep the current at a certain value. How to control the current to a constant value according to the characteristics of the resonant circuit has become the primary task of the converter control algorithm.

A. MATHEMATICAL MODEL OF THE RESONANT CONVERTER IN CURRENT OPERATION MODE

The circuit structure of the resonant converter is shown in Figure 2, the equivalent circuit diagram can be made when it starts to work in current source mode by combing with its working principle and usage of T-type equivalent circuit model (see Figure 7).

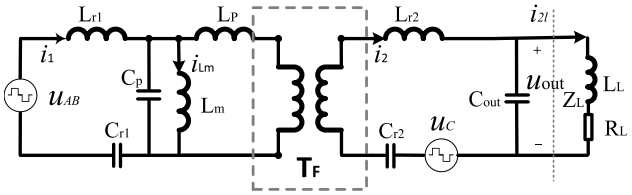

FIGURE 7. Equivalent circuit diagram of resonant converter combined with reverse current control.

In Figure 7, L_P is the primary inductance of the isolation transformer and L_m is the magnetizing inductance. The above two parameters are all converted to the primary side. L_{r1} and C_{r1} are form the primary resonance circuit, L_{r2} and C_{r2} are form the secondary resonance circuit. Combined with the current reverse control method stated above, the circuit can be divided into two parts, one part is the secondary side circuit is not in conduction area which is shown in Figure 8a, another part is the secondary side circuit is in conduction area as shown in Figure 8b. The direction of transformer's secondary side voltage and LC resonance voltage's direction is shown in Figure 8a. Comparing Figure 8b with 8a, the direction of the two voltages has been changed since the IGBTs are working in conduction area α. To simplify the analysis, set the transformer transformation ratio to 1: 1. According to the working principle of the resonant converter, in order to improve the efficiency, the resonant converter generally works near the resonance frequency point, and the current waveform is approximately sinusoidal. Under this situation, the resonant converter is equivalent to a linear network to analyze its input and output characteristics. Meantime, assuming that the voltage $u_2 + u_{LC2}$ in secondary side after entering the conduction region α is uniformly expressed by u_c.

When a short-circuit fault occurs, according to the working principle of reverse current control, the controllable output voltage source u_c is used in the equivalent circuit of Figure 8 to illustrate the control function. If the resonant circuit works normally to transmit power, u_c does not work and its output voltage is zero. By using the principle of superposition, it needs to find out the effect of the output voltage u_{AB} on

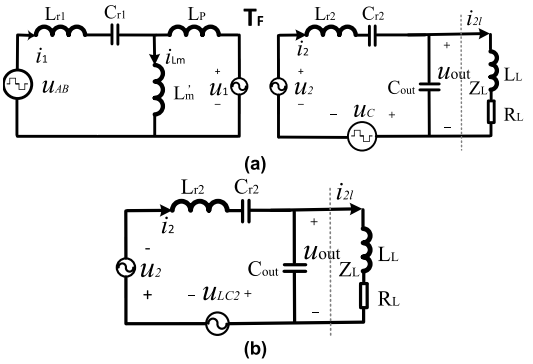

FIGURE 8. Equivalent circuit diagram of resonant converter when considering reverse current control. (a) Equivalent circuit without reverse control. (b) Equivalent circuit with reverse control.

the output current in the primary-side using phase-shifting control. It can be concluded that the relationship between the output current i_{2l1} and the primary-side voltage u_{AB} is:

$$H(j\omega_s) = \frac{i_{2l1}}{u_{AB}} = \frac{\frac{Z_m}{z_{r2}+z_L}}{z_{r1}+\frac{Z_m}{z_{r2}+z_L}} \cdot \frac{z_L}{z_{r2}+z_{eq}} \cdot \frac{1}{z_L} \tag{3}$$

Here ω_s is the switching angular frequency. Equation (3) can be obtained after the simplification:

$$\begin{aligned} H(j\omega_s) = \omega_s L_m / [&\left(\omega_s L_{r1} - \frac{1}{\omega_s C_{r1}} + \omega_s L_m\right)(\omega_s L_L + R_L) \\ &+ j(\omega_s^2 L_{r1} L_m - \frac{L_m}{C_{r1}} \\ &+ \omega_s^2 L_{r2} L_m - \frac{L_m}{C_{r2}} + \omega_s^2 L_{r1} L_{r2} \\ &- \frac{L_2}{C_{r1}} + \frac{1}{\omega_s^2 C_{r1} C_{r2}} - \frac{L_{r1}}{C_{r2}}) \end{aligned} \tag{4}$$

The imaginary part of the denominator at resonance is 0, that is:

$$\begin{aligned} \omega_s^2(L_{r1}L_m + L_{r2}L_m + L_{r1}L_{r2}) - \frac{L_m}{C_{r1}} - \frac{L_m}{C_{r2}} - \frac{L_2}{C_{r1}} \\ - \frac{L_{r1}}{C_{r2}} + \frac{1}{\omega_s^2 C_{r1} C_{r2}} = 0 \end{aligned} \tag{5}$$

Then the relationship between the output current i_{2L} and the primary side inverter phase shift control voltage u_{AB} is:

$$i_{2l1} = \frac{\omega_s L_m}{\left(\omega_s L_{r1} - \frac{1}{\omega_s C_{r1}} + \omega_s L_m\right)(\omega_s L_L + R_L)} \cdot u_{AB} \tag{6}$$

When the short circuit occurs, u_c starts to work, and the relationship between this voltage and the output current i_{2L} can be derived as follows:

$$i_{2l2} = \frac{\omega_s C_{r2}}{j\left(\omega_s^2 L_{r2} C_{r2} - 1 + \omega_s^2 L_L C_{r2}\right) + (\omega_s C_{r2} R_L)} \cdot u_C \tag{7}$$

Similarly, in resonance situation, the part of $\omega_s^2 L_{r2} C_{r2} - 1$ the denominator is 0, then:

$$i_{2l2} = \frac{1}{j(\omega_s L_L) + R_L} \cdot u_C \tag{8}$$

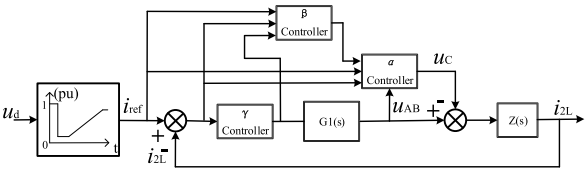

FIGURE 9. Block diagram of short-circuit current controller.

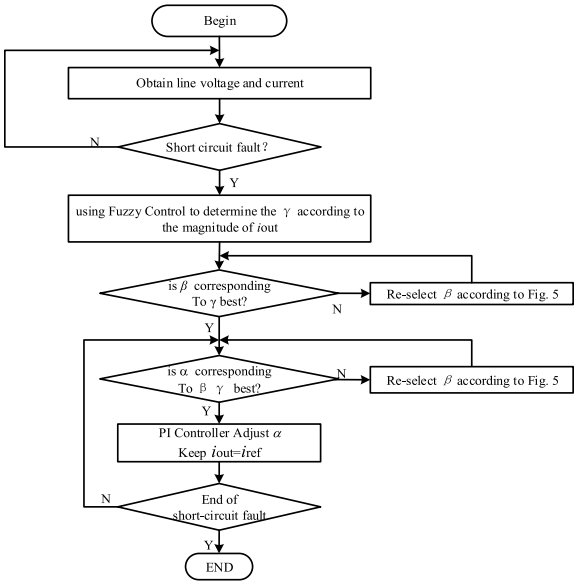

FIGURE 10. The control strategy program flow chart.

Combining these above two parts, considering the control voltage direction, output current i_{2L} is achieved after the current reverse control is introduced when in short circuit:

$$\begin{aligned} i_{2l} = &\frac{\omega_s L_m}{\left(\omega_s L_{r1} - \frac{1}{\omega_s C_{r1}} + \omega_s L_m\right)(\omega_s L_L + R_L)} \cdot u_{AB} \\ &- \frac{1}{j(\omega_s L_L) + R_L)} \cdot u_C \end{aligned} \tag{9}$$

It can be seen from (9) that the output current of the transformer during the short circuit is related to two parts, one part is the phase shift control voltage u_{AB} on the primary rectification side of the transformer which involves the phase shift control angle γ at primary side. The other is related to the control voltage u_c. The size of u_c is related to the control lagging angle β and conduction angle α, which brings a lot of flexibility. Of course, the control will be more complicated.

B. OUTPUT CURRENT REVERSE CONTROL METHOD

The number of phase shift variables to control output current from resonance converter has increased from one to three by introducing a current reverse control strategy. Of course, lagging angle β and conduction angle α on the inverter side is finally reflected by the control voltage u_c. Therefore, designing of a reasonable control strategy is vital to result a maximum advantage by using these three control quantities.

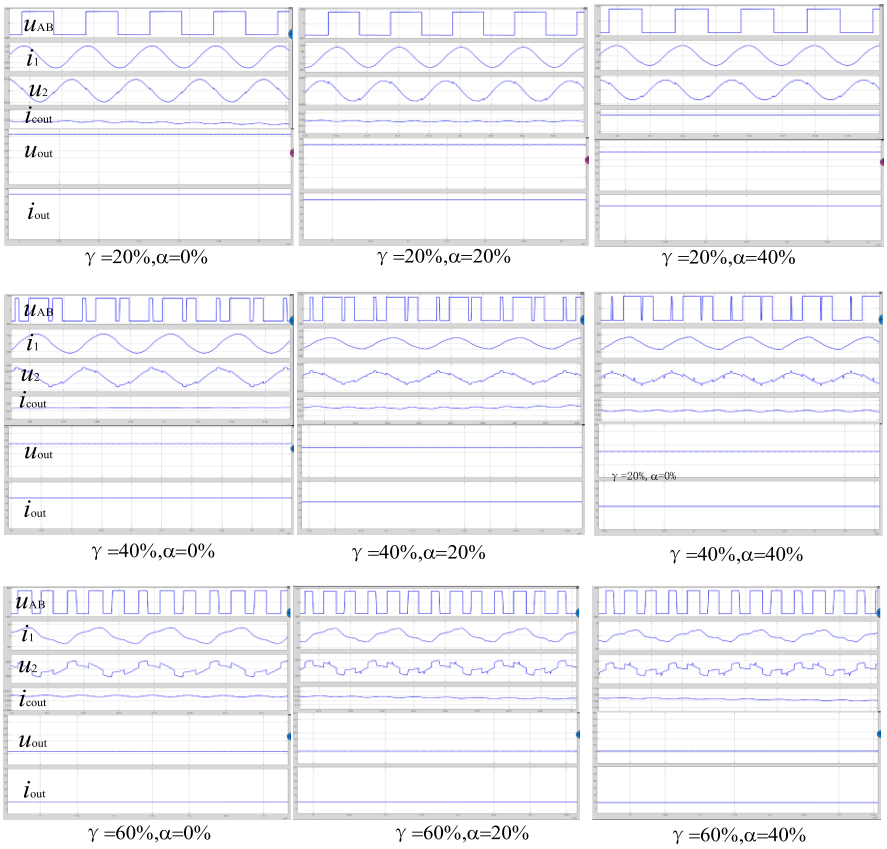

FIGURE 11. Simulation results on different inverse phase angle γ and conduction angle α.

The basic idea of the design is to use the pre-decision speed of fuzzy control and to make full use of the good following control performance of PI controller. According to the current reference value during low voltage ride through and the partition where γ is located, the primary side voltage u_{AB} is determined first, then determine whether there is a suitable conduction width (angle α) to ensure that there is enough adjustment interval. Next, determine whether the lagging angle β is in the range with the best linearity. When all these conditions are met, the control angle α is adjusted to realize the change of the output current of the converter according to the required value. Due to the uncertainty of the location of the short circuit, these quantities are not static. In the early stage, the control effect can be optimized through the combination with actual engineering and through self-learning and self-adaptive on-site parameters. The structured block diagram of the designed control system is shown in Figure 9.

G1(s) is the transfer function of converter's secondary side, Z(s) is the line impedance when short circuit situation happens.

$$G1(s) = \frac{\omega_s L_m}{\left(\omega_s L_{r1} - \frac{1}{\omega_s C_{r1}} + \omega_s L_m\right)} \tag{10}$$

$$Z(s) = \frac{1}{(\omega_s L_L) + R_L)} \tag{11}$$

The control algorithm is realized in dSPACE platform. According to the system control requirements, when a short-circuit fault occurs on the external line, line voltage ud decreases rapidly, controller will set the reference current according to the low voltage ride through requirement basing on the real measurement voltage. Due to the uncertain location of the short circuit, the output voltage of converter will also change from high to low with the distance of the short circuit location. From the characteristic curve of low voltage ride through, it can be seen that the output current required at this time will vary with the magnitude of the short circuit voltage. Such characteristic output requires the controller to have good tracking control ability. According to the fuzzy PI control strategy, control program flow chart is shown in Figure 10.

V. SIMULATION AND EXPERIMENTAL VERIFICATION

According to the analysis results in the article, the working conditions of the resonant converter at different angles of γ, α and β are simulated through simulation to verify the possibility and rationality of the control method. In-depth understanding of the impact of the conduction angle α on the output voltage of the resonant converter at different con-

duction widths. Figure 11 shows the simulation results of different inverter phase shift angle γ and conduction angle α.

It can be seen from the figure that as the inverter phase shift angle γ and conduction angle α change, the output voltage and current will also decrease, and the current can be effectively controlled. Corresponding to each inverse transform phase angle γ, the conduction angle α can be fine-tuned. It shows that through the control cooperated between these three angles, the control amount can be made more precisely and meet the requirements of current control in higher precision.

In order to verify the above short-circuit current reverse control algorithm, a hardware-in-the-loop experimental system based on dSPACE and Plecs RT box platform was built. The experimental platform is shown in Figure 12, and above circuit topology and control method are comprehensively verified on this platform. Table 1 shows the main parameters of the circuit.

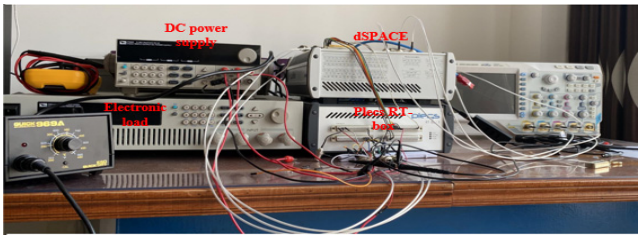

FIGURE 12. Hardware-in-the-loop experiment system.

Figure 13 shows the output voltage and current experimental waveforms of several groups of circuits with different inverse phase angle γ and conduction angle α, which verifies the correctness of the control method described above. Figure 13a is the experimental waveform when phase shifting angle $\gamma = 40\%$, lagging angle $\beta = 20\%$ and inverted conduction angle $\alpha = 40\%$. Figure 13b is the experimental waveform when phase shifting angle $\gamma = 40\%$, lagging angle $\beta = 20\%$ and inverted conduction angle $\alpha = 20\%$. Figure 13c is the experimental waveform when phase shifting angle $\gamma = 20\%$, lagging angle $\beta = 20\%$ and inverted conduction angle $\alpha = 40\%$.

TABLE 1. List of main parameters of resonant converter.

U_{in}	1000V	n	2：1
L_{r1}	20.5μH	L_{r2}	40μH
C_{r1}	100nF	C_{r2}	750nF
L_m	1000μH	C_{out}	100μF

Figure 14 shows the operation of the CLLC module output in the DC transformer based on different short-circuit output current reference values. Seeing from Figure 14a, when output current changes from a relatively large value to a small value, current controller can finish this procedure within 2-3 resonance periods, which indicates a good current control

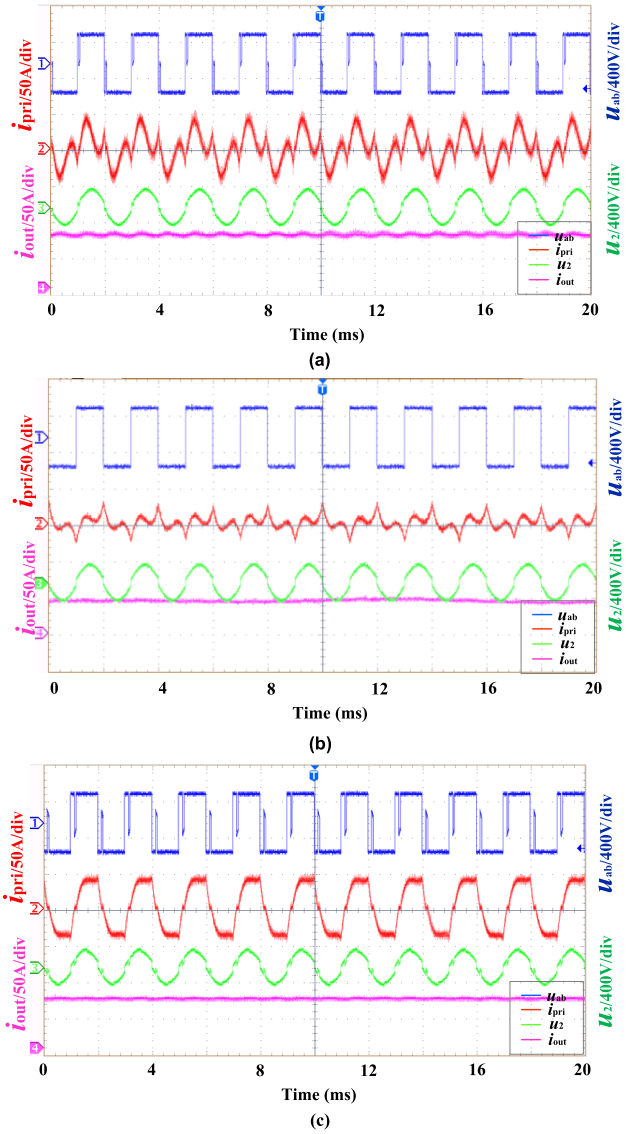

FIGURE 13. Experimental waveforms of the output voltage and current of the resonant converter circuit. (a) Experimental results with $\gamma = 40\%$, $\beta = 20\%$ and $\alpha = 40\%$. (b) Experimental results with $\gamma = 40\%$, $\beta = 20\%$ and $\alpha = 20\%$. (c) Experimental results with $\gamma = 20\%$, $\beta = 20\%$ and $\alpha = 40\%$.

performance. Figure 14b is showing the current controller controlling the output current according to the predetermined output current. The current waveform changes uniformly, reflecting that the controller has good following control performance. Figure 14c is the process of the controller controlling the current from small to large value, which the output current curve changes smoothly.

It can be seen from the figure that facing to different output voltages when short circuit happen, the transformer can satisfy the requirements of stabilized output current thus can full fill the function of low voltage ride though.

VI. CONCLUSION

The CLLC type resonant conversion circuit can satisfy the operating conditions of ZVS and ZCS in most of the output

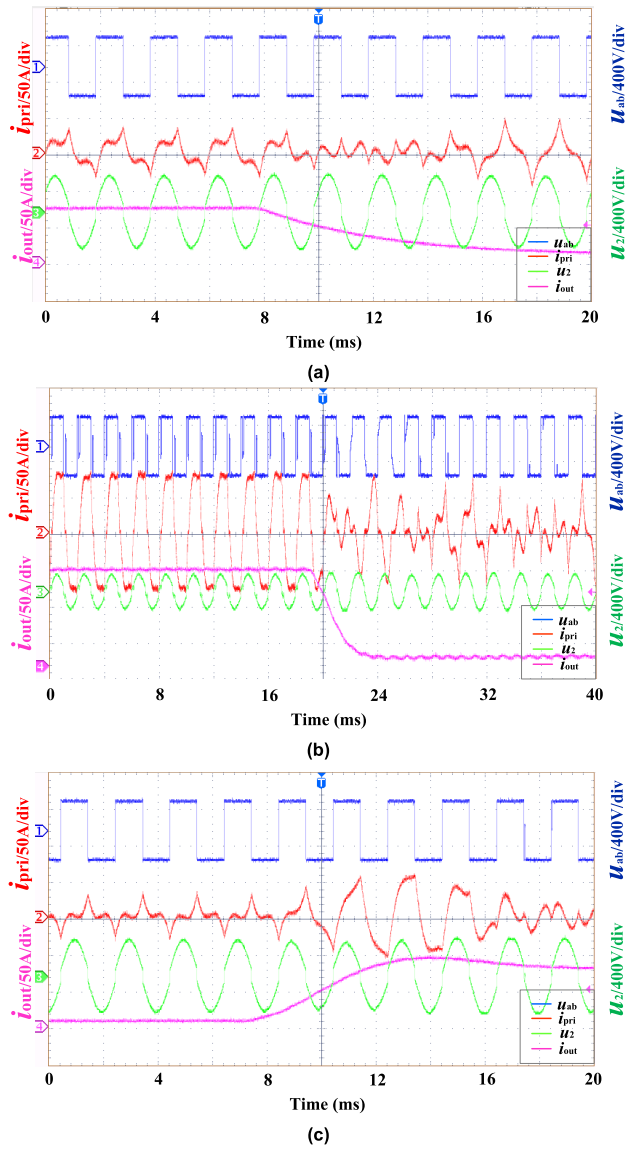

FIGURE 14. Experimental results of dynamic changes of output current with different settings. (a) γ angle remains unchanged and the output current drops by 50%. (b) γ angle remains unchanged and the output current drops by 100%. (c) γ angle remains unchanged and the output current rises 50%.

power range. The DC transformer based on this type of converter has high efficiency and is widely valued, especially as grid connected interface device for renewable energy source of DC distribution networks. To meet the requirements of low-voltage ride-through for the function of grid-connected power generation equipment, the current control characteristics must be studied. By analyzing the working principle of the circuit, this article proposes a reverse current control method, which can expand the output current control sensitivity of the DC transformer under the condition of short circuit fault of the external line. Through the phase shift control angle of the primary inverter, and the secondary side rectification, the control between the conduction angle of the bridge and the angle difference between the primary and secondary sides enables the DC transformer to meet the requirements of controlling its output current according to its port voltage when the line short circuit occurs. Simulation analysis and hardware In-loop experiments verified the correctness of the proposed method.

REFERENCES

[1] K. Sano and M. Takasaki, "A surgeless solid-state DC circuit breaker for voltage-source-converter-based HVDC systems," *IEEE Trans. Ind. Appl.*, vol. 50, no. 4, pp. 2690–2699, Jul./Aug. 2014.

[2] L. Chen, L. Tarisciotti, A. Costabeber, F. Gao, P. Wheeler, and P. Zanchetta, "Advanced modulations for a current-fed isolated DC–DC converter with wide-voltage-operating ranges," *IEEE J. Emerg. Sel. Topics Power Electron.*, vol. 7, no. 4, pp. 2540–2552, Dec. 2019.

[3] Z. Saadatizadeh, P. C. Heris, M. Sabahi, and E. Babaei, "A DC–DC transformerless high voltage gain converter with low voltage stresses on switches and diodes," *IEEE Trans. Power Electron.*, vol. 34, no. 11 pp. 10600–10609, Nov. 2019.

[4] Y. Xuan, X. Yang, W. Chen, T. Liu, and X. Hao, "A novel NPC dual-active-bridge converter with blocking capacitor for energy storage system," *IEEE Trans. Power Electron.*, vol. 34, no. 11, pp. 10635–10649, Nov. 2019.

[5] H. Kunlun, C. Zexiang, and L. Yang, "Study on protective performance of HVDC transmission line protection with different types of line fault," in *Proc. 4th Int. Conf. Electr. Utility Deregulation Restructuring Power Technol. (DRPT)*, Weihai, Shandong, 2011, pp. 358–361, doi: 10.1109/DRPT.2011.5993917.

[6] H. Li, W. Li, M. Luo, A. Monti, and F. Ponci, "Design of smart MVDC power grid protection," *IEEE Trans. Instrum. Meas.*, vol. 60, no. 9, pp. 3035–3046, Sep. 2011.

[7] A. Gomez-Exposito, J. M. Mauricio, and J. M. Maza-Ortega, "VSC-based MVDC railway electrification system," *IEEE Trans. Power Del.*, vol. 29, no. 1, pp. 422–431, Feb. 2014.

[8] H. Chen, X. Wu, and S. Shao, "A current-sharing method for interleaved high-frequency LLC converter with partial energy processing," *IEEE Trans. Ind. Electron.*, vol. 67, no. 2, pp. 1498–1507, Feb. 2020.

[9] K.-C. Tseng, S.-Y. Chang, and C.-A. Cheng, "Novel isolated bidirectional interleaved converter for renewable energy applications," *IEEE Trans. Ind. Electron.*, vol. 66, no. 12, pp. 9278–9287, Dec. 2019.

[10] S. Lumbreras and A. Ramos, "Optimal design of the electrical layout of an offshore wind farm applying decomposition strategies," *IEEE Trans. Power Syst.*, vol. 28, no. 2, pp. 1434–1441, May 2013.

[11] P. Hu, R. Yin, Z. He, and C. Wang, "A modular multiple DC transformer based DC transmission system for PMSG based offshore wind farm integration," *IEEE Access*, vol. 8, pp. 15736–15746, 2020, doi: 10.1109/ACCESS.2019.2962620.

[12] C. Zhuo, X. Zhang, X. Zhang, and X. Yang, "Current status and development of fault current limiting technology for DC transmission network," in *Proc. IEEE 10th Int. Symp. Power Electron. Distrib. Gener. Syst. (PEDG)*, Jun. 2019, pp. 306–310.

[13] S. A. Assadi, H. Matsumoto, M. Moshirvaziri, M. Nasr, M. S. Zaman, and O. Trescases, "Active saturation mitigation in high-density dual-active-bridge DC–DC converter for on-board EV charger applications," *IEEE Trans. Power Electron.*, vol. 35, no. 4, pp. 4376–4387, Apr. 2020.

[14] T. Todorcevic, R. van Kessel, P. Bauer, and J. A. Ferreira, "A modulation strategy for wide voltage output in DAB-based DC–DC modular multilevel converter for DEAP wave energy conversion," *IEEE J. Emerg. Sel. Topics Power Electron.*, vol. 3, no. 4, pp. 1171–1181, Dec. 2015.

[15] X. Wang, J. Liu, S. Ouyang, T. Xu, F. Meng, and S. Song, "Control and experiment of an H-bridge-based three-phase three-stage modular power electronic transformer," *IEEE Trans. Power Electron.*, vol. 31, no. 3, pp. 2002–2011, Mar. 2016.

[16] H.-S. Lee and J.-J. Yun, "Quasi-resonant voltage doubler with snubber capacitor for boost half-bridge DC–DC converter in photovoltaic micro-inverter," *IEEE Trans. Power Electron.*, vol. 34, no. 9, pp. 8377–8388, Sep. 2019.

[17] B. Li, Q. Li, and F. C. Lee, "High-frequency PCB winding transformer with integrated inductors for a bi-directional resonant converter," *IEEE Trans. Power Electron.*, vol. 34, no. 7, pp. 6123–6135, Jul. 2019.

[18] J. Tian, D. Hu, C. Zhou, Y. Yang, W. Wu, C. Mao, and D. Wang, "Individual DC voltage balance control for cascaded H-bridge electronic power transformer with separated DC-link topology," *IEEE Access*, vol. 7, pp. 38558–38567, 2019, doi: 10.1109/ACCESS.2019.2905006.

[19] W. Lin and D. Jovcic, "Average modelling of medium frequency DC–DC converters in dynamic studies," *IEEE Trans. Power Del.*, vol. 30, no. 1, pp. 281–289, Feb. 2015.
[20] G. J. Kish, M. Ranjram, and P. W. Lehn, "A modular multilevel DC/DC converter with fault blocking capability for HVDC interconnects," *IEEE Trans. Power Electron.*, vol. 30, no. 1, pp. 148–162, Jan. 2015.
[21] J.-W. Shin, M. Ishigaki, E. M. Dede, and J. S. Lee, "MagCap DC–DC converter utilizing GaN devices: Design consideration and quasi-resonant operation," *IEEE Trans. Power Electron.*, vol. 34, no. 3, pp. 2441–2453, Mar. 2019.
[22] M. Rashidi, N. N. Altin, S. S. Ozdemir, A. Bani-Ahmed, and A. Nasiri, "Design and development of a high-frequency multiport solid-state transformer with decoupled control scheme," *IEEE Trans. Ind. Appl.*, vol. 55, no. 6, pp. 7515–7526, Nov./Dec. 2019.
[23] N. B. Chagas and T. B. Marchesan, "Analytical calculation of static capacitance for high-frequency inductors and transformers," *IEEE Trans. Power Electron.*, vol. 34, no. 2, pp. 1672–1682, Feb. 2019.
[24] L. F. Costa, G. Buticchi, and M. Liserre, "Optimum design of a multiple-active-bridge DC–DC converter for smart transformer," *IEEE Trans. Power Electron.*, vol. 33, no. 12, pp. 10112–10121, Dec. 2018.
[25] S. Du, B. Wu, K. Tian, D. Xu, and N. R. Zargari, "A novel medium-voltage modular multilevel DC–DC converter," *IEEE Trans. Ind. Electron.*, vol. 63, no. 12, pp. 7939–7949, Dec. 2016.
[26] C. Sun, X. Cai, J. Zhang, and G. Shi, "Suppression of reactive power in isolated modular multilevel DC–DC converter under quasi square-wave modulation," *IEEE Access*, vol. 7, pp. 23940–23950, 2019, doi: 10.1109/ACCESS.2019.2899158.
[27] Z. Guo and K. Sun, "Three-level bidirectional DC–DC converter with an auxiliary inductor in adaptive working mode for full-operation zero-voltage switching," *IEEE Trans. Power Electron.*, vol. 33, no. 10, pp. 8537–8552, Oct. 2018.
[28] C. Wang, L. Yang, Y. Wang, and B. Chen, "A 1-kW CLTCL resonant DC–DC converter with restricted switching loss and broadened voltage range," *IEEE Trans. Power Electron.*, vol. 33, no. 5, pp. 4190–4203, May 2018.
[29] B. Zhao, Q. Song, J. Li, X. Xu, and W. Liu, "Comparative analysis of multilevel-high-frequency-link and multilevel-DC-link DC–DC transformers based on MMC and dual-active bridge for MVDC application," *IEEE Trans. Power Electron.*, vol. 33, no. 3, pp. 2035–2049, Mar. 2018.
[30] Y. Wang, Z. Wang, J. Fan, Y. Guan, Y. Xie, S.-Z. Chen, G. Zhang, and Y. Zhang, "Adaptive modulation strategy for modular multilevel high-frequency DC transformer in DC distribution networks," *IEEE Access*, vol. 8, pp. 16397–16408, 2020, doi: 10.1109/ACCESS.2020.2967177.
[31] M. Pahlevani, S. Eren, H. Pahlevaninezhad, I. Askarian, and S. Bagawade, "Digital current sensorless control of current-driven full-bridge DC/DC converters," *IEEE Trans. Power Electron.*, vol. 33, no. 2, pp. 1797–1815, Feb. 2018.
[32] S. Li, Q. Min, E. Rong, R. Zhang, X. Du, and S. Lu, "A magnetic integration half-turn planar transformer and its analysis for LLC resonant DC–DC converters," *IEEE Access*, vol. 7, pp. 128408–128418, 2019, doi: 10.1109/ACCESS.2019.2939274.
[33] M. S. Bhaskar, M. Meraj, A. Iqbal, S. Padmanaban, P. K. Maroti, and R. Alammari, "High gain transformer-less double-duty-triple-mode DC/DC converter for DC microgrid," *IEEE Access*, vol. 7, pp. 36353–36370, 2019, doi: 10.1109/ACCESS.2019.2902440.

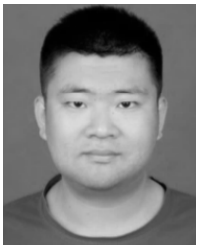

CHAORAN ZHUO (Member, IEEE) was born in Xi'an, China, in 1990. He received the B.S. degree from the Fontys University of Applied Sciences, in 2013, and the M.S. degree in electrical engineering from the Eindhoven University of Technology, Eindhoven, The Netherland, in 2016. He is currently pursuing the Ph.D. degree with the Power Electronics and Renewable Energy Center, Xi'an Jiaotong University, Xi'an.

He is also with the State Key Laboratory of Electrical Insulation and Power Equipment, School of Electrical Engineering, Xi'an Jiaotong University. His current research interests include DC–DC converter, power electronic transformer, and current limiting control technology of power electronic equipment.

XU YANG (Senior Member, IEEE) received the B.S. and Ph.D. degrees in electrical engineering from Xi'an Jiaotong University, Xi'an, China, in 1994 and 1999, respectively.

Since 1999, he has been a member of the faculty of the School of Electrical Engineering, Xi'an Jiaotong University, where he is currently a Professor. From November 2004 to 2005, he was with the Center of Power Electronics Systems, Virginia Polytechnic Institute and State University, Blacksburg, VA, USA, as a Visiting Scholar. He then came back to Xi'an Jiaotong University and was involved in the teaching and research in power electronics and industrial automation area. His research interests include soft-switching topologies, pulse width modulation control techniques and power electronic integration, and packaging technologies.

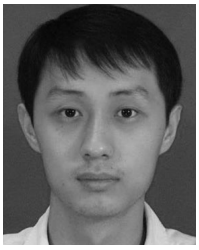

XIAOTIAN ZHANG (Member, IEEE) was born in Xi'an, China, in 1983. He received the B.S. (Hons.) and M.S. degrees in electrical engineering from Xi'an Jiaotong University, Xi'an, in 2006 and 2009, respectively, and the Ph.D. degree (Hons.) in electrical engineering and electronics from the University of Liverpool, Liverpool, U.K., in 2012.

Until 2015, he was with the Department of Electrical Engineering, Imperial College London, London, U.K. He is currently an Associate Professor with the Department of Electrical Engineering, Xi'an Jiaotong University. His research interests include control and design of HVDC converters.

XIONG ZHANG was born in Xi'an, China, in 1992. He received the B.S. degree in electrical engineering from the University of Central Lancashire, in 2014, and the master's degree in embedded system technology from the University of Sussex, U.K., in 2016. He is currently pursuing the Ph.D. degree with the School of Electrical Engineering, Xi'an Jiaotong University.

His main research fault current analysis of DC power grid and fault current limiters of HVDC systems.